

Original paper

Fluid inclusion study of the Horní Luby cinnabar deposit, Saxothuringian Zone, Bohemian Massif: clues for the metamorphic remobilization of mercury

Dalibor VELEBIL¹, Jiří ZACHARIÁŠ^{2*}

¹ Department of Mineralogy and Petrology, National Museum in Prague, Cirkusová 1740, 193 00 Prague 9, Czech Republic; dalibor.velebil@nm.cz

² Institute of Geochemistry, Mineralogy and Mineral Resources, Charles University in Prague, Albertov 6, 128 43 Prague 2, Czech Republic; jiri.zacharias@natur.cuni.cz

* Corresponding author



The stratiform deposit of mercury at Horní Luby near Cheb (Czech Republic) is hosted by Ordovician phyllites of Vogtland–Saxony Paleozoic Unit in the Saxothuringian Zone of the Bohemian Massif. Ore is represented by cinnabar disseminated within the phyllite and by lenticular bodies rich in massive cinnabar (lenses with a thickness of up to 1 m and length along the strike varying from less than 1 m up to 20 m). Cinnabar is accompanied by pyrite and locally also siderite. The P–T history of the mineralization was deciphered by the study of fluid inclusions. Early fluids are represented by a homogenous H₂O–CO₂ fluid trapped in secretion quartz. This fluid underwent several heterogenization events starting from approximately 300 °C and continued down to 200–150 °C. Metamorphic quartz of secretion origin crystallized at ~300 °C, while hydrothermal pyrite crystallized at 220–210 °C and cinnabar at 195–160 °C. The formation of the richest ore was associated with the replacement of metamorphic quartz in phyllites by the cinnabar in weakly alkaline solutions.

The cinnabar is pure phase, free of admixtures (Bi, Sb, Zn, Fe, and Cu). It is accompanied by minute blebs of Hg-bearing sphalerite (11–12 wt. % Hg) that might indicate earlier presence of the zincian metacinnabar and more complex metamorphic history of the ore. The primary source of mercury is thought to be Lower Paleozoic submarine volcanism. The formation of ore bodies is, however, associated with metamorphic mobilization of mercury during the late stages of the Variscan orogeny.

Despite being relatively small, the mercury deposit at Horní Luby competed with the mines in Idrija (Slovenia) and Almadén (Spain) in the 16th century. The production of mercury at Horní Luby is estimated to have corresponded to c. 10–30 % of the mercury production in the mines of Idrija and Almadén at that time. In addition to Venice, the mercury from Horní Luby was also supplied to Nürnberg, Antwerp and Lyon. In 1520–1540, the production of mercury from the Horní Luby mines was 6 to 15 tons per annum. The mines were abandoned in 1597. Attempts to reinstitute mining activity in the 17th, 18th and 19th centuries were not very extensive and always failed. The total production of the Horní Luby mines during the whole mining history is estimated to have been at least 200 tons of mercury. Much of this amount was extracted between 1520 and 1540, with a minor portion between 1560–1570.

Keywords: cinnabar, mercury, fluid inclusions, Horní Luby, Saxothuringian Zone, Bohemian Massif

Received: 5 November 2012; **accepted:** 11 September 2013; **handling editor:** D. Dolejš

1. Introduction

Mercury mineralization is associated with nearly all geological epochs, starting with the Archean, till recent times (e.g. Hazen et al. 2012). The most important mercury deposits, however, were formed during the last 430 Ma. They are represented by two distinctive classes: i) sequences of marine sediments rich in organic matter that underwent thermal mobilization by volcanic or intrusive activity, or by metamorphic processes (e.g. the two largest mercury deposits – Almadén in Spain and Idrija in Slovenia; Saupé 1990; Jébrak and Hernandez 1995; Hernández et al. 1999; Lavrič and Spanberg 2003; or great number of small deposits – e.g. Akçay et al.

2006; Martín-Izard et al. 2009) and ii) epithermal deposits like the silica–carbonate deposits formed during hydrothermal alteration and replacement of serpentinite bodies (< 5.3 Ma in age; New Almadén and New Idria in California, USA; e.g. Studemeister 1984; Smith et al. 2008), as well as numerous hot-spring mercury deposits worldwide (e.g. White 1981; Hampton et al. 2004).

Typical temperatures of mercury ore formation span a range from c. 200 °C down to 100 °C, or even less. Some deposits underwent metamorphic reworking; among them the Levigliani and Ripa deposits in the Apuane Alps, Italy are the best-studied examples (Dini et al. 2001). Part of mercury in the past was also recovered from other deposit types, e.g. from hydrothermal vein-type mineralization

(commonly represented by Hg-rich tetrahedrite) and associated with fluids of complex/metamorphic origin.

About 40 occurrences of mercury minerals have been reported from the territory of the Czech Republic (e.g. Chrt and Strnad 1961; Chrt 1972; Sattran 1980; Chrt 2001); however only five of them were rich enough to be intermittently mined during the 14th to 19th centuries. Two of these deposits are hosted by unmetamorphosed Ordovician sedimentary and volcanosedimentary sequences of the Barrandian Basin (Jedová hora u Hořovic, Svatá u Berouna), while the three others are associated with metamorphosed shales of Neoproterozoic, Cambrian–Ordovician and Silurian ages (Bezdrůžice near Mariánské Lázně, Jesenný by Semily and Horní Luby by Cheb). The studied Horní Luby deposit in the Saxothuringian Zone was the most important among them, having yielded c. 300 t of Hg. This paper is aimed to summarize data relevant to the genetic model of this deposit.

2. History of mercury mining at the Horní Luby ore district

The beginning of mining of cinnabar near Luby is usually dated to the 13th or 14th century (e.g. Löwl 1908). A ruling by the Holy Roman Emperor and Czech King Charles IV, according to which tax had to be paid on cinnabar transported from Western Bohemia. (Kořan 1942), provides indirect evidence for mercury mining in this region in the 14th century. The first unambiguous document confirming mining at Luby dates back to the second half of the 15th century; however, mining of cinnabar at Horní Luby peaked in the 16th century, especially its first half. A number of archive parameters are available from that time, describing the progress of local mining in detail (Klier 1969; Bílek et al. 1978a). The mercury deposit in Horní Luby is relatively small; nonetheless, in the first half of the 16th century it competed with the other mercury mines in Europe. It has been estimated that the production of mercury at Horní Luby corresponded to 10 to 30 % of the production of the mercury mines in Idrija or Almadén at that time (Klier 1969). In fact, in 1525 to 1527, the miners in Idrija repeatedly managed prohibition of the transport of Czech mercury across the Alps to the important sales area in Venice. In addition to Venice, mercury from Horní Luby was also supplied to Nürnberg, Antwerp and Lyon (Klier 1969; Bílek et al. 1978a).

In the 16th century, six mines were in operation at Horní Luby. The main were the Annunciation of the Virgin Mary (*Maria Verkündigung*) and Three Kings (*Drei König*) mines, consisting of five shafts over an area with dimensions of about 300 × 300 m. Further, less important mines in the close vicinity of Horní Luby included the Help of God (*Hilfe Gottes*), Feud of Count Šlik (*Graf*

Albrecht Schlicken Lehen), *Gendorf* and *Pernhaut* mines. All of them were operated by rich burghers and traders from Nürnberg and also, but fewer, from Jáchymov.

In 1520–1540, the mercury production at Horní Luby varied between 6 and 15 t p.a., from 1560 to 1570 decreased to between 0.5 and 3 t p.a. Between 1520 and 1570, the accessible upper parts of the main section of the deposit (the Annunciation of the Virgin Mary and Three Kings mine complex) were exhausted to a depth of 50 to 100 m, after which mining declined and the mines were abandoned in 1597. Mining was performed for a short time in the Feud of Count Šlik mine in the 1620's. This mine was again renewed in 1676 to 1681 and in 1810.

Various entrepreneurs expressed interest in the Horní Luby Hg deposit in 1892 to 1939, but no great activity occurred. Geological prospecting took place at the deposit and its surroundings in 1956 to 1962 (Kulnig et al. 1963), in the context of which a 77 m deep exploration shaft was bored directly at Horní Luby, from which three exploration tunnels branched out at a depth of 65 m, with a total length of 400 m, searching for, and partly following, the cinnabar ore deposit.

The total production of the mining area over its entire history has been estimated as at least 200 tons of Hg, whereby most of this amount was extracted in 1520–1540 and a lesser amount in 1560–1570; sporadic mining at later times was negligible. History of mercury mining and metallurgy at Horní Luby was recently summarized by Velebil (2009).

3. Geological setting

3.1. Regional geology

The Saxothuringian Zone of the European Variscan Belt can be subdivided into metamorphosed crystalline core complexes of the Erzgebirge–Fichtelgebirge (Fig. 1a) and the unmetamorphosed to weakly metamorphosed Paleozoic complexes (to the northwest). Five tectonic units were distinguished in the Erzgebirge core (e.g. Konopásek and Schulmann 2005): 1) paraautochthonous unit, 2) two HP–HT gneiss units with eclogites, 3) HP–LT mica schist unit with eclogites, 4) MP–LT unit of garnet-bearing phyllites and 5) LP–LT phyllic unit. The metamorphic grade generally decreases from the central part (northeast) to the southwest, west and north (Lorenz 1989).

The LP–LT phyllite unit gradually passes into low-grade slates and, further to the west (northwest), into unmetamorphosed Paleozoic sediments. The LP–LT unit, together with the unmetamorphosed sediments, is therefore also referred to as the Vogtland–Saxonian Paleozoic Unit. Several sequences were identified therein:

Frauenbach Beds, Phycodes Formation and Gräfenthal Formation. The Paleozoic complex probably originated during the Late Cambrian to Early Ordovician crustal extension along a passive continental margin (Falk et al. 1995). Frauenbach Beds contain chlorite–sericite phyllites (bearing ample albite) with abundant quartzite and quartzitic phyllite intercalations. Graphitic layers, metalydites and quartzites represent characteristic intercalations of the Phycodes Formation (phyllites). The basement of the Paleozoic complex represent micaceous schists and gneisses.

The Paleozoic complex was metamorphosed at *c.* 200–300 MPa and 300 °C (Rötzler et al. 1998). Metadiabase sills from the Kraslice area (about 30 km NW of Horní Luby), hosted by the LP–LT phyllite unit, contain relics of alkali amphiboles crystallized at 350–400 °C and 600–700 MPa (Holub and Souček 1992). The peak of the HP–LT stage (1.4 GPa at 460 °C) preserved in chloritoid-bearing phyllites of the (garnet)-phyllite unit must be older than 360 Ma cooling ages of phengitic white mica (Faryad and Kachlík 2013).

The Paleozoic sequences are characterized by relatively flat-lying foliation, with WNW–ESE trending stretching lineation and fold axes. They were intruded by Carboniferous plutons – the Nejdeč–Eibenstock Pluton to the NE and the Smržiny (Fichtelgebirge) Pluton to the SW. The contact-metamorphic zone (andalusite hornfelses) of the Nejdeč–Eibenstock Pluton is *c.* 200–500 m wide.

The most important ore mineralization types associated with the Paleozoic sequences are the syngenetic Beshi-type sulphidic ores from the Kraslice district (Pertold et al. 1994), the stratiform to epigenetic Hg-mineralization (Horní Luby) and sparse epigenetic Pb–Zn quartz–carbonate vein type mineralization (Oloví district and some other occurrences). The Horní Luby deposit is the only mercury deposit in the region; several other cinnabar occurrences, mostly fracture-related, are known from the broader vicinity in Germany: near Erlbach (in phyllites; Scheufele 1940), at Niederhasslau (in quartzite), at Loitzsch hosted by Ordovician shales (Schulz 1965) and from various hydrothermal quartz veins at Bockwa, Hartenstein and Gera (Tischendorf 1989). In the Czech Republic, they appear at Opatov and Výspa (Sattran et al. 1978), Trojmezí (Chrt 2001), Hranice and Studenec (Chrt 1972, 2001).

Maucher (1976) reported several small cinnabar deposits in eastern Alps (Austria). These ore deposits (Glatschach, Hohes Kohr, Rottrasten, Stockenboi, Eisenkappel and Vellacher Kotschna) are hosted in Ordovician–Silurian metamorphic sequences (phyllites and quartzites interbedded with mafic metavolcanics) and show textural–structural features very similar to Horní Luby and Levigliani deposits.

3.2. Geology of the Horní Luby ore district

The deposit is hosted by the Frauenbach Beds, close to the base of the Phycodes Formation (Fig. 1b). Sattran et al. (1978) suggested Lower Ordovician age of phyllites in the Horní Luby area, while Chrt (2001) assumed Upper Cambrian age. In relation to metamorphism, the deposit is located within the LP–LT phyllic unit, close to its boundary with the MP–LT unit (garnet-bearing phyllites).

The ore body is hosted by chlorite–sericite phyllites and by muscovite quartzites. Metamorphic foliation strikes WNW–ESE and dips 10–30° to NNE (Chrt and Strnad 1961; Sattran and Škvor 1962). Phyllites contain numerous lenses of secretion quartz; some also siderite. Metabasites are relatively rare in the studied area (Sattran et al. 1978); however, they become more frequent towards the NW and especially in the vicinity of Kraslice (Holub and Souček 1992; Pertold et al. 1994).

The Frauenbach Beds at Horní Luby form a weakly undulating syncline. The syncline is dissected by several transversal NNW–SSE striking normal faults, among which the most prominent is the Luby Fault. The western block subsided along this fault by *c.* 100 m relative to the eastern one (Sattran and Škvor 1962). Another noticeable fault of this system is located to the west of Horní Luby (Sattran et al. 1978). The principal part of the ore deposit (together with all the historical mines) is localized between these two major faults. The system of subvertical faults striking E–W and NE–SW is subordinate (Kulnig et al. 1963). The Luby Fault is over 30 km long and even displaces Tertiary sediments of the Cheb Basin.

Historical mine workings are completely inaccessible and the dumps were recultivated many years ago. Description of the geology of the deposit is therefore largely based on a few published papers and many unpublished reports. According to Bílek et al. (1978a) the oldest descriptions of the ore were given by Bittner and by Count Pötting in 1786 and in 1810, respectively. Exploration activities carried during 1958–1962 were summarized by Kulnig et al. (1963). Chrt (1972, 2001), Sattran (1980) and Sattran et al. (1978) combined the data of Kulnig et al. (1963) with their own information from regional geological mapping and exploration.

3.2.1. Cinnabar ore bodies

Cinnabar mineralization is mostly disseminated, less frequently vein-related. The disseminated mineralization is conformable with the metamorphic foliation (S_1). Cinnabar-rich ore lenses (< 1 m thick and < 20 m along the strike) are also parallel with the S_1 foliation planes. The contact between these ore lenses and weakly mineralized host-rock is transitional. Ore lenses (striking

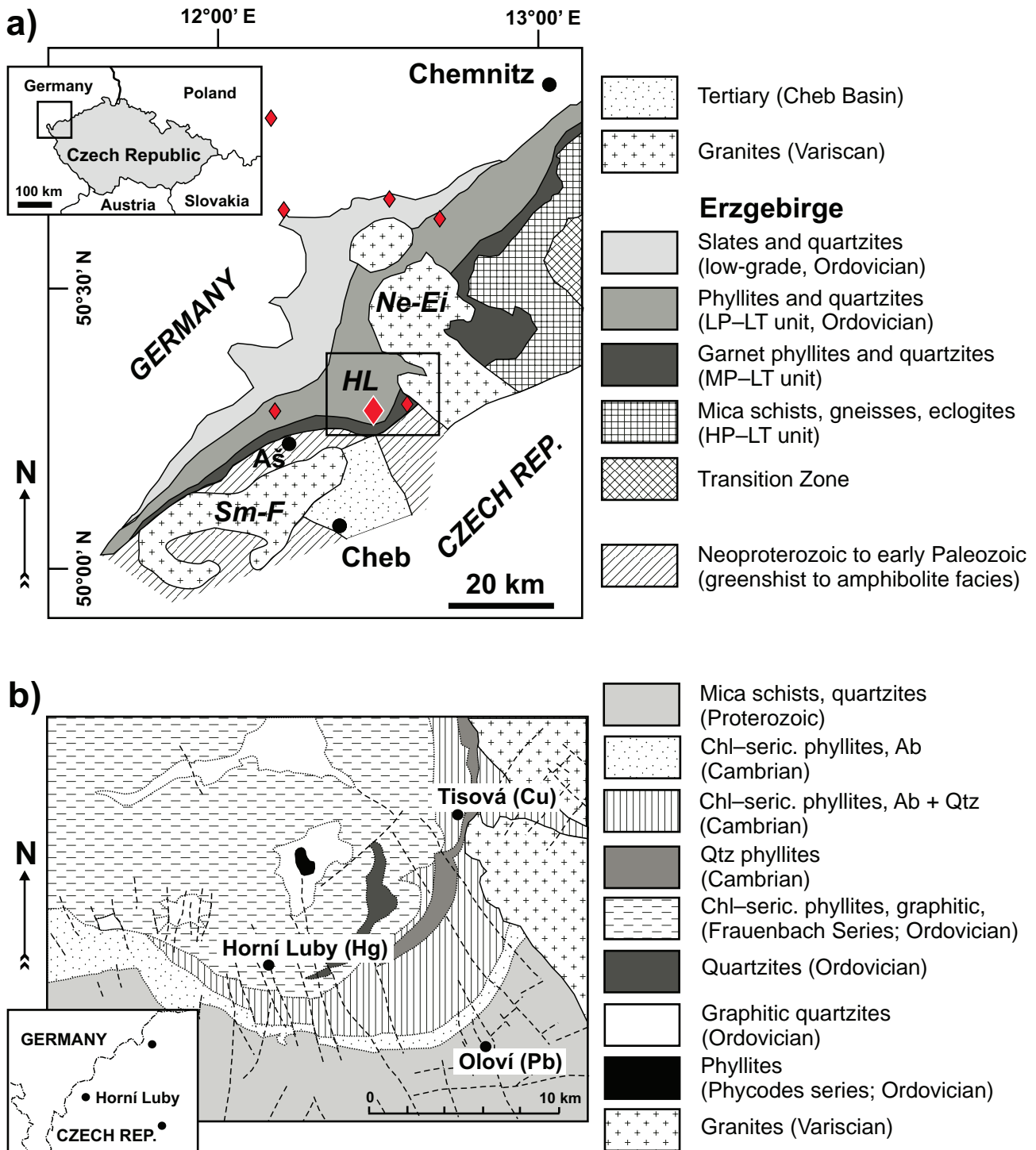


Fig. 1a – Geological scheme of the Western Erzgebirge region. Occurrences of mercury mineralization are marked by diamonds. Abbreviations: Ne-Ei = Nejedek–Eibenstock Pluton, Sm-F = Smrčiny–Fichtelgebirge Pluton, HL = Horní Luby; **b** – Geological map of the Horní Luby area.

WNW–ESE, dipping 10–30° to NNE) occur in several parallel horizons (Satran et al. 1978). Locally, the ore was localized in fold hinges, especially at the Feud of Count Šlik mine (Pötting 1810 in Bílek et al. 1978b). Cleavage planes (S_2), inclined at about 15° with respect

to the S_1 foliation, are intensively coated by limonite, but are free of cinnabar (Chrt and Strnad 1961).

In total, four ore lenses with macroscopic cinnabar ore were identified in the exploration adit during 1961–1962. The size of the largest one was about 10 × 5 × 0.3 m and

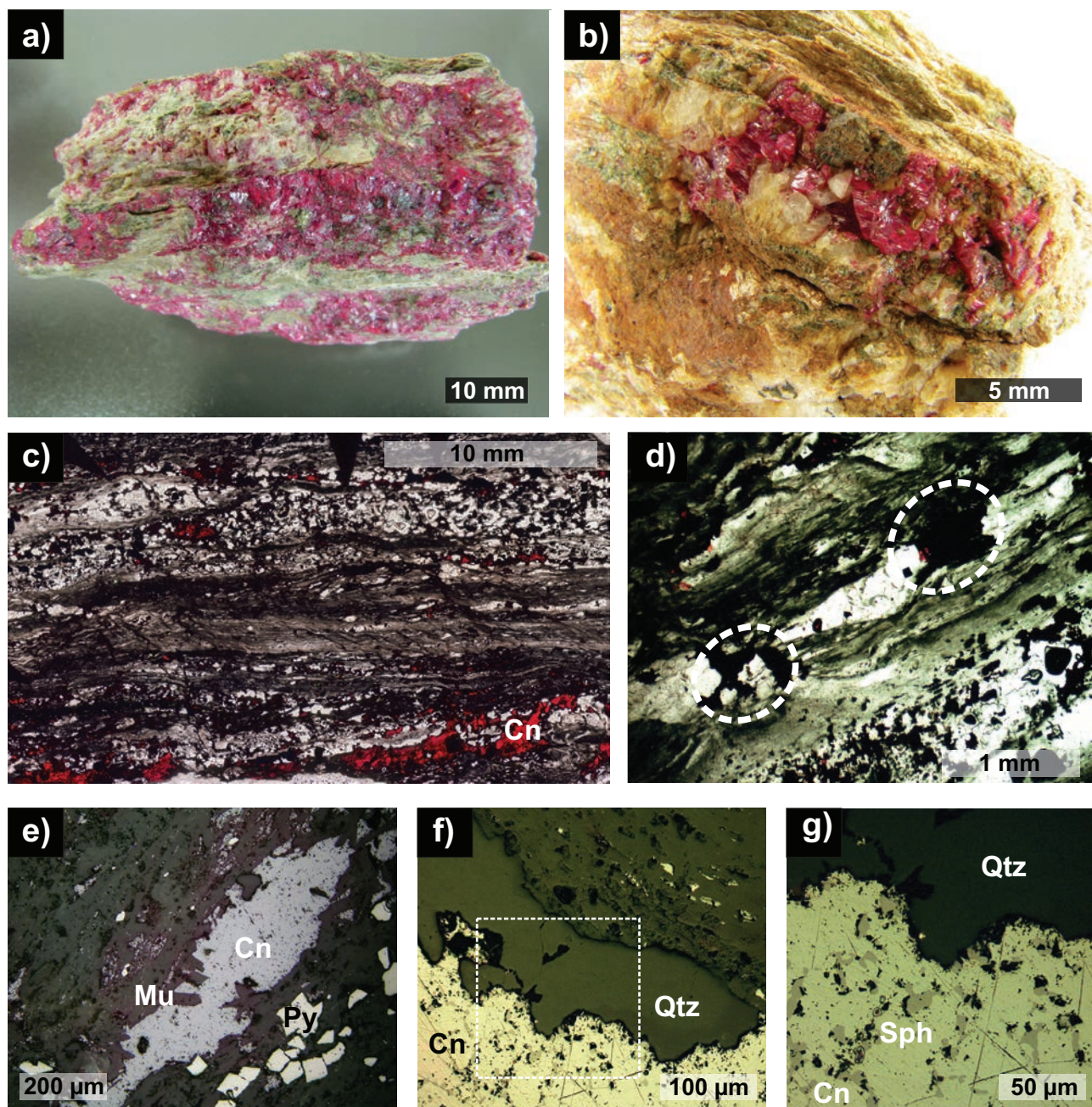


Fig. 2 Macro photos and photomicrographs of the studied cinnabar ores: **a** – phyllite with disseminated cinnabar; **b** – phyllite with primary drusy cavity filled by cinnabar; **c** – phyllite with disseminated cinnabar (Cn) and pyrite (Py); **d** – the richest cinnabar accumulations apparently fill necks (highlighted by white dashed ellipses) within the quartz-rich band of the phyllite; **e** – crystals of metamorphic sericitic muscovite (Mu) overgrown by cinnabar; **f** – irregular contact between quartz (Qtz) and cinnabar suggesting dissolution of the former by the latter; **g** – detail of the previous photo; small blebs of medium-grey sphalerite (Sph) are enclosed in cinnabar. These blebs tend to be more frequent towards the cinnabar–quartz boundary.

contained 270 t of ore at 0.13 wt. % Hg. In total, 351 kg of mercury were recovered during exploration activities (Kulnig et al. 1963).

In addition to disseminated mineralization (Fig 2a), cinnabar also fills fractures in the lenses of metamorphic secretion quartz (Fig. 2b). Chrt and Strnad (1961) also encountered veinlets (up to only several mm thick) of

massive cinnabar crosscutting both the metamorphic foliation and the secretion quartz lenses.

3.2.2. Mineralogy

Chrt and Strnad (1961) distinguished three morphological types of cinnabar mineralization with unknown mutual re-

relationships: i) disseminated mineralization in phyllite (from the oldest to the youngest phase: pyrite → quartz → cinnabar); ii) disseminated mineralization in quartzite (quartz carbonate → cinnabar) and iii) fracture-related mineralization in metamorphic secretion quartz (quartz → cinnabar).

They also suggested significant metasomatic replacement of metamorphic rock-forming quartz (in phyllite) by cinnabar or first by carbonate and then by cinnabar (in quartzite). Cinnabar is always the youngest ore phase, pyrite the oldest one (Chrt and Strnad 1961; Kulnig et al. 1963; Sattran et al. 1978).

Disseminated pyrite is by far more abundant and more widespread in phyllites than the cinnabar. Pyrite may

thus represent older mineralization, not associated with cinnabar (Chrt and Strnad 1961).

4. Methods

The present study is based on a detailed mineralogical and fluid-inclusion study of ore samples from mineralogical collection of the National Museum, Prague. In total 6 double polished wafers, each about 200–250 μm thick, were prepared for the fluid inclusion study. Fluid-inclusion petrography was conducted using a Leica DMPL microscope (magnification up to 1000×), fluid inclusion

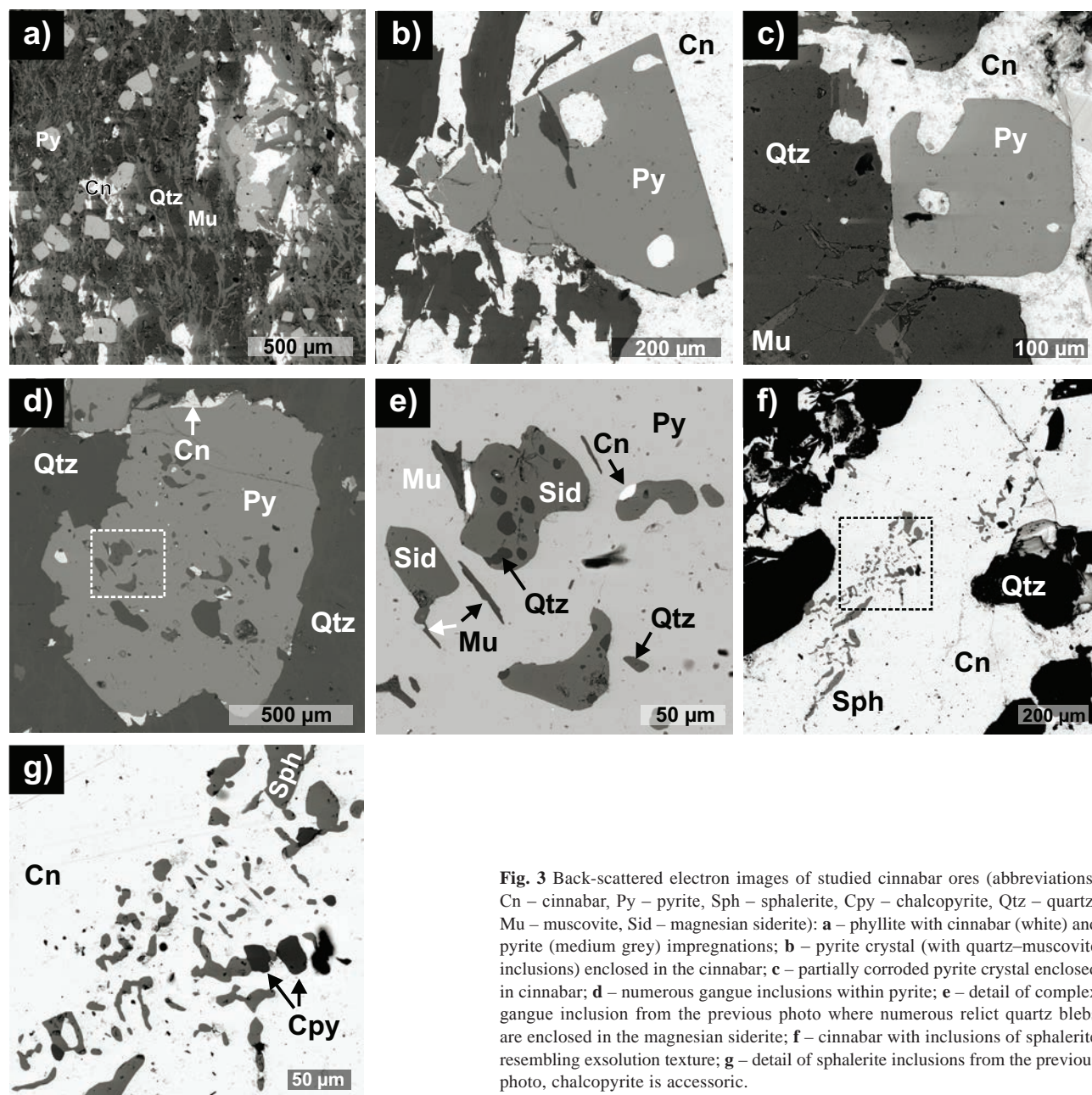


Fig. 3 Back-scattered electron images of studied cinnabar ores (abbreviations: Cn – cinnabar, Py – pyrite, Sph – sphalerite, Cpy – chalcopyrite, Qtz – quartz, Mu – muscovite, Sid – magnesian siderite): **a** – phyllite with cinnabar (white) and pyrite (medium grey) impregnations; **b** – pyrite crystal (with quartz–muscovite inclusions) enclosed in the cinnabar; **c** – partially corroded pyrite crystal enclosed in cinnabar; **d** – numerous gangue inclusions within pyrite; **e** – detail of complex gangue inclusion from the previous photo where numerous relict quartz blebs are enclosed in the magnesian siderite; **f** – cinnabar with inclusions of sphalerite resembling exsolution texture; **g** – detail of sphalerite inclusions from the previous photo, chalcopyrite is accessory.

microthermometry using the Linkam THMSG 600 heating–freezing stage and Olympus BX-40 microscope with 50× ULWD objective. The stage was calibrated using synthetic and natural standards, and the precision of the measurements is ± 0.1 °C from -50 °C to $+ 50$ °C and ± 3 °C above 300 °C.

Microthermometric data were collected only for carefully selected fluid-inclusion assemblages. The measured phase transitions included the melting temperature of the last ice crystal (T_m -ice), the melting temperature of solid CO_2 (T_m - CO_2), the temperature of CO_2 -clathrate dissociation (T_m -Clath), the temperature of CO_2 homogenization (T_h - CO_2) and the total homogenization temperature (T_h -tot). Homogenization occurred mostly to the liquid (L), rarely to the vapor (V) or via a critical mode (C). The degree of fill (F) is estimated as the $L/(V + L)$ ratio at 30 °C. Salinities were calculated as wt. % eq. NaCl using the equations of Bodnar (1993) for aqueous fluids and Bakker (1997, 1999) for aqueous–carbonic fluids. The salinity of aqueous–carbonic fluids includes correction for the admixture of CH_4 . The data of Thiery et al. (1994) were used to estimate the composition and molar volume of the gaseous phase in terms of the binary CO_2 - CH_4 mixture. The isochores were calculated by the equations of Zhang and Frantz (1987) and Bakker (1999) for the H_2O -salt and H_2O - CO_2 - CH_4 -NaCl systems, respectively.

Additional 10 samples (polished thin sections and polished cut slabs) were studied by standard or ore microscopy and by electron microscope techniques. The mineral chemistry was obtained using an energy dispersive X-ray (EDX) analyzer (X-Max by Oxford Instruments, operated by M. Racek) mounted on the Vega-Tescan scanning-electron microscope at the Faculty of Science, Charles University in Prague. The composition of cinnabar was also checked by the Cameca SX 100 microprobe (WDS mode) at the Masaryk University, Brno (operated by R. Škoda; accelerating voltage 25 kV, beam current 20 nA, beam size 1 μm). The standards used (Cameca SX 100): native Ag ($\text{Ag } L_\alpha$), chalcopyrite ($\text{S } K_\alpha$), native Sb ($\text{Sb } L_\beta$), galena ($\text{Pb } M_\alpha$), native Bi ($\text{Bi } M_\beta$), CdTe ($\text{Cd } L_\beta$), HgTe ($\text{Hg } M_\alpha$), pyrite ($\text{Fe } K_\alpha$), Co ($\text{Co } K_\alpha$), pararammelsbergite ($\text{Ni } K_\alpha$, $\text{As } L_\beta$), native Cu ($\text{Cu } K_\alpha$), PbSe ($\text{Se } L_\beta$) and ZnS ($\text{Zn } K_\alpha$).

5. Description of studied samples

5.1. Phyllite with disseminated cinnabar mineralization

Studied phyllite sample (5×4 cm) exceptionally rich in cinnabar consists of alternating illite (“sericite”)-rich and quartz-rich bands, up to ~5 mm thick each (Fig. 2c–d).

The illite-rich bands are fine-grained and contain, in addition to illite, quartz, chlorite, pyrite and cinnabar (Figs 2–3). Pyrite (30–500 μm) is mostly euhedral (cubes) and predominates over anhedral cinnabar (30–500 μm). All minerals, including cinnabar and pyrite, grew syntectonically in metamorphic foliation (S_1). Younger cleavage planes (S_2) lack any ore or metamorphic–retrograde minerals.

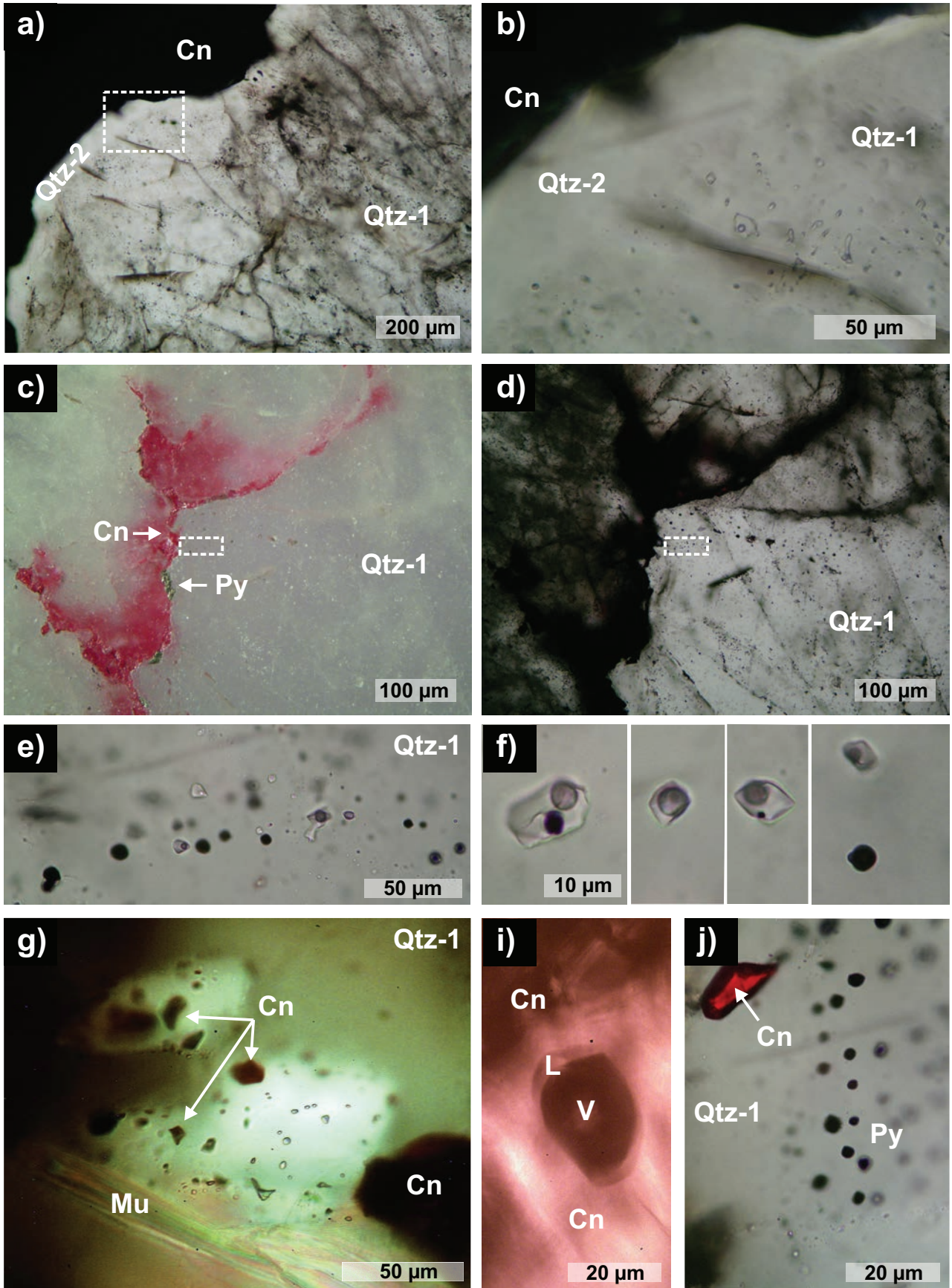
Quartz rich bands contain coarse-grained (up to 2 mm) quartz and pyrite. Quartz ribbons are rimmed by illite (“sericite”). Euhedral to subhedral pyrite occasionally hosts minute inclusions of quartz, illite or chloritoid (?). The grain boundaries between cinnabar and pyrite are straight (i.e. metamorphic), or highly irregular (Fig. 3c–d), suggesting pyrite dissolution by cinnabar-bearing fluids (or by fluids preceding cinnabar deposition). Cinnabar aggregates (up to 2 mm in size) fill cracks in quartz-rich ribbons or, more frequently, replace these ribbons (Fig. 2f–g).

Occasionally, we have found textural evidence for the occurrence of older corroded quartz with cinnabar microinclusions on its surface, overgrown by younger quartz (Fig. 4g). The younger quartz, although also in contact with the cinnabar, lacks any signs of corrosion. This might indicate that quartz dissolution occurred mostly at the early mineralization stage (i.e. disseminated mineralization in phyllite) and not during the late stage (formation of fracture-related cinnabar). This conclusion is supported by the absence of any quartz dissolution in the secretion quartz (see below).

5.2. Metamorphic-secretion quartz with fracture-related mineralization

Massive milky quartz (Qtz-1) from a quartz lens, c. 30 mm thick, contains cinnabar on some fractures approximately perpendicular to the S_1 foliation. Individual quartz grains are up to 4–5 mm in size, mostly anhedral and exhibit weak undulatory extinction. Quartz contains sparse primary and numerous secondary cavities. Secondary cavities resulted from supergene leaching of pyrite aggregates. Primary, i.e. crystallization-related, cavities are rimmed by a zone of transparent drusy quartz (crystals up to 3 mm long; Qtz-2). The transparent quartz (Qtz-2) also forms a narrow discontinuous rim (Fig. 4a–b) along the ore phases (pyrite or cinnabar) and the quartz gangue (Qtz-1). The transparent quartz is therefore younger than the milky quartz.

Cinnabar fills primary cavities or fractures in the massive quartz (Qtz-1). It is accompanied by pyrite and by accessory muscovite, chlorite and siderite (always as the youngest phase). We have found no textural evidence for quartz replacement by cinnabar in this type of mineralization.



Tab. 1 Electron-microprobe analyses of selected ore phases from the Horní Luby mercury deposit

Sample	Lb723	Lb723	Lb723	LB-1	LB-1	LB-1	LB-1
Analyzed by	EDX	EDX	EDX	WDX	WDX	WDX	WDX
Mineral	Sphalerite	Sphalerite	Cinnabar	Cinnabar	Cinnabar	Cinnabar	Cinnabar
Zn (wt. %)	57.1	58.3	n.d.	n.d.	n.d.	n.d.	n.d.
Hg (wt. %)	12.1	10.9	86.4	86.19	86.47	86.07	85.40
S (wt. %)	30.1	30.6	14.0	13.52	13.75	13.69	13.61
Total (wt. %)	99.3	99.8	100.5	99.71	100.22	99.76	99.02
Zn (a.p.f.u.)	0.93	0.94	–	–	–	–	–
Hg (a.p.f.u.)	0.06	0.06	0.99	1.009	1.003	1.002	1.001
S (a.p.f.u.)	1.00	1.00	1.01	0.991	0.997	0.998	0.999
Total (a.p.f.u.)	2.00	2.00	2.00	2.000	2.000	2.000	2.000

5.3. Comments on the ore mineralogy

Image analysis of the mineralized phyllite sample identified the following mineral proportions (in areal %): cinnabar (4–7 %), pyrite (5–10 %), chlorite (14–20 %), muscovite (18–25 %), quartz and feldspar (~50 %). We found no differences in the chemistry of ore minerals between the mineralized phyllite and secretion quartz samples. Pyrite always exhibited stoichiometric composition with no identifiable trace-element admixture. Similarly, the cinnabar is a stoichiometric phase (Tab. 1), free of any impurities (contents of Ag, Zn were just at/below the detection limits). Identified minor phases corresponded to sphalerite and chalcopyrite, both typically less than 50 µm in size. Sphalerite inclusions in the cinnabar locally resemble an exsolution texture (Fig. 3f–g), or occur as blebs along the pyrite–cinnabar boundaries. Sphalerite always exhibits an admixture of mercury (~11–12 wt. % Hg; Tab. 1), while the Zn content in the cinnabar is always below the detection limit of 0.20 wt. %. There is a positive correlation between Hg and Zn contents in the ore (Fig. 5). Hydrothermal carbonate coexisting with the cinnabar was identified as magnesian siderite ($\text{Fe}_{0.498}\text{Mg}_{0.415}\text{Mn}_{0.071}\text{Ca}_{0.009}\text{Zn}_{0.007}$).

↔

Fig. 4 Optical-microscope photos of fluid-inclusion assemblages (for mineral abbreviations, consult the previous figure): **a** – the contact between the massive milky quartz (Qtz-1) and fracture-hosted ore (cinnabar) is rimmed by a narrow zone of transparent inclusion-free quartz of the second generation (Qtz-2); **b** – detail of the previous photo; inclusion-free Qtz-2 rim in contrast to numerous two-phase inclusions within the Qtz-1; **c** – quartz-grain boundaries discontinuously rimmed by cinnabar and pyrite (reflected light). The grain boundaries served as conduits for late migration of ore-bearing fluids; **d** – same as previous photo but with transmitted light. Quartz contains numerous primary and secondary fluid inclusions; **e** – detail of the two previous photos; secondary trail with simultaneously trapped ore (pyrite) and fluid inclusions; **f** – details of several three-phase fluid inclusions with accidentally trapped ore phase (pyrite); **g** – simultaneously trapped ore (cinnabar) and fluid inclusions “wetting” surface of partially corroded grains of Qtz-1; **h** – two-phase vapor-rich fluid inclusion enclosed in the cinnabar; **i** – trail of secondary inclusions dominated by ore inclusions (pyrite >> cinnabar).

6. Fluid inclusions

Three types of fluids were identified: 1) $\text{H}_2\text{O}-\text{CO}_2 > \text{CH}_4$ -salt (type I); 2) $\text{CO}_2 \gg \text{CH}_4 \gg \text{H}_2\text{O}$ (type II); and 3) H_2O -salt (type III). Highly variable liquid to gas ratio is a common feature associated with the type I inclusions. Many of the studied fluid-inclusion assemblages are thus suspected of being trapped from a heterogeneous fluid. Gaseous inclusions (type II) are much less frequent and most probably represent an isolated product of heterogenization of the $\text{H}_2\text{O}-\text{CO}_2$ fluid. Microthermometric data for type I and II inclusions are very similar and are thus presented together. Fluid inclusions, irrespective of type, are typically less than 20 µm across and oval. In addition to fluid inclusions, microinclusions of ore minerals are frequent in some samples (sometimes trapped alongside with fluid inclusions).

6.1. Fluid inclusions in the metamorphic secretion quartz

Massive quartz contains numerous trails of secondary inclusions. We have found frequently unambiguous textural evidence for simultaneous trapping of the pyrite (mostly), cinnabar (less frequently) and a fluid. Ore phases were identified by optical microscopy, by microprobe (EDX) and also checked by micro Raman spectroscopy. The size and shape of the ore inclusions is similar to those of the associated fluid inclusions. Ore inclusions trails (\pm fluid) typically occur in the immediate vicinity of larger to macroscopic ore phases, hosted either by fractures, or by primary cavities. The ore trails thus most probably represent tensional micro-cracks associated with the formation of macroscopic fractures.

In total, 11 fluid-inclusion assemblages were measured (see below and Tab. 2):

Assemblages 1, 2 and 3 represent three mutually parallel secondary trails hosted by milky quartz (Qtz-1). One trail contained only type III inclusions, while the other two trails hosted mixed type I and II inclusions. Trapping from a heterogeneous phase is therefore

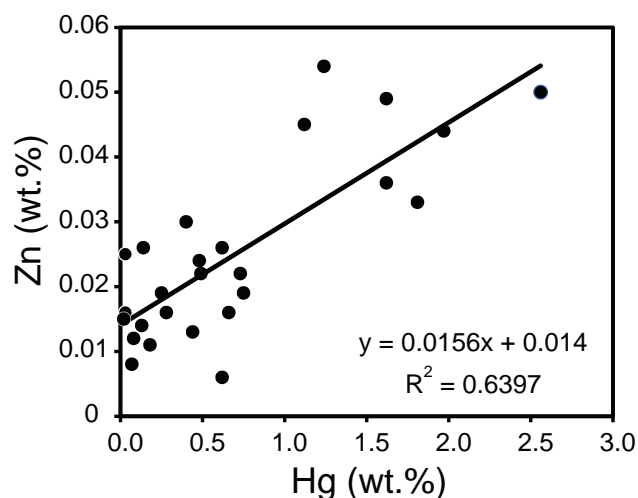


Fig. 5 Correlation between the contents of Hg and Zn in ore samples from exploration shaft at Horní Luby (sampled in 1962), based on data of Sattran et al. (1978).

probable. The homogenization temperature of type III inclusions (~160 °C) was interpreted as the trapping temperature.

Assemblages 4, 5 and 6 (type III) are all hosted by a narrow rim of transparent quartz (Qtz-2) along the contact with a large pyrite aggregate (fracture-hosted). Fluid inclusions form short intracrystalline trails or are randomly 3D-distributed; this might indicate their pseudo-secondary origin. We suggest that they reflect the conditions of ore phase formation.

Assemblages 7, 8 and 9 represent randomly distributed clusters of type I and type III inclusions hosted by the milky quartz (Qtz-1).

Assemblage 10 (Qtz-1) is exceptional in the presence of dark circular two-phase solid inclusions (up to 30 µm in size, typically only 5–10 µm) with pyrite in the core and with organic matter forming the outer shell. Occasionally CO₂ or H₂O–CO₂ > CH₄–salt (type II or I) volumetrically minor fluid phase was found attached to some of these solid inclusions. Type I inclusion with the lowest degree of fill (F = 0.15) homogenized to a vapor at about 220 °C. This temperature may thus represent the trapping temperature of this unusual assemblage.

Assemblage 11a (Qtz-1) represents a secondary trail with pyrite microinclusions interspersed with common aqueous-only (type III) and occasional gaseous (type II) inclusions. Type III inclusions seem to be co-genetic with pyrite inclusions. This is supported by an occurrence of type III fluid inclusions with an accidentally trapped pyrite (Fig. 3f).

Assemblage 11b (type III) represents a secondary trail that is clearly younger than trail 11a. *Assemblage 11c* (type I) crosscuts trail 11a and might be older in origin than trails 11a and 11b.

6.2. Fluid inclusions in phyllite with disseminated cinnabar mineralization

Fluid inclusions in the rock-forming quartz from phyllite are mostly monophasic aqueous (liquid H₂O; type III),

Tab. 2 Summary of studied fluid-inclusion assemblages

#:(¹)	Type	F(²)	T _m -CO ₂ (°C)	(Td-Cl _a) T _m -ice (°C)	Th-CO ₂ (L + V = L) (°C)	Th-tot(³) range (°C)	Th-tot(⁴) avg ± std (n) (°C)
1	H ₂ O–CO ₂	0.0–0.5	–56.6	(9.9)	13.1 to 30.5		–
2	H ₂ O–CO ₂	0.1–0.4	–56.6	(9.8)	27.7 to 30.5		–
3	H ₂ O	0.95		–2.9		167.5 (L)	167.5 (1)
4a	H ₂ O	0.90		–1.1 to –1.2		148–166 (L)	161.3 ± 5.9 (8)
4b	H ₂ O	0.90		–3.5		208–224 (L)	215.8 ± 5.7 (9)
5	H ₂ O	0.90		–3.4		181–182 (L)	181.5 ± 0.5 (2)
6	H ₂ O	0.95		–2.2		192–196 (L)	194.1 ± 3.1 (2)
7	H ₂ O	0.90		–3.3		186–215 (L)	202.2 ± 11.6 (6)
8	H ₂ O	0.95		n.m.		171–180 (L)	177 ± 5.3 (3)
9a	CO ₂	0	–57.1		26.8 to 28.4		–
9b	H ₂ O–CO ₂	0.0–0.2	–56.8 to –56.9	(9.1 to 8.2)	22.7 to 28.2		–
9c	H ₂ O	0.75	–57.0				259.3 (L)
10	H ₂ O	0.95		–0.7 to –1.6		153–162 (L)	157.9 ± 4.4 (3)
11a	H ₂ O	0.90		–2.4		203–232 (L)	218.5 ± 11.6 (4)
11b	H ₂ O–CO ₂	0.0–0.6	–56.9 to 57.0	(9.2)	24.9 to 29.5	220 (V)	
11c	H ₂ O	0.6–0.9		–3 to –2	(11 & 18.4)	192 (D)	
		0.90		–3 (?)		207–215 (L)	210.9 ± 5.2 (2)
				–2 to –1.8		214.1 (L)	
		0.95		(9.0 to 9.3)	23.6 to 24.4	168–172 (L)	169.1 ± 2.5 (3)
		0.80	–57.4			285 (C)	
						>300	

Notes: (¹) fluid inclusion assemblage number (see text for detailed description); (²) degree of fill; (³) temperature of total homogenization (L ... to liquid, V ... to vapor, C ... critical mode, D ... decrepitation of inclusion before its homogenization); (⁴) mean ± 1 standard deviation (number of data is given in brackets)

less frequently monophasic carbonic (liquid CO₂; type II) or, rarely, two/three phase aqueous-carbonic (H₂O–CO₂; type I). Inclusions are highly variable in size (3–60 μm), mostly oval or suboval in shape. Monophasic inclusions (II, III) usually wet grain boundaries, rarely occur isolated inside quartz grains, or form short secondary trails. No extensive fluid inclusion trails that would crosscut several grain boundaries were found. All the inclusions can be classified as synmetamorphic/syntectonic ones. Microthermometric data were collected for inclusions type I and II only.

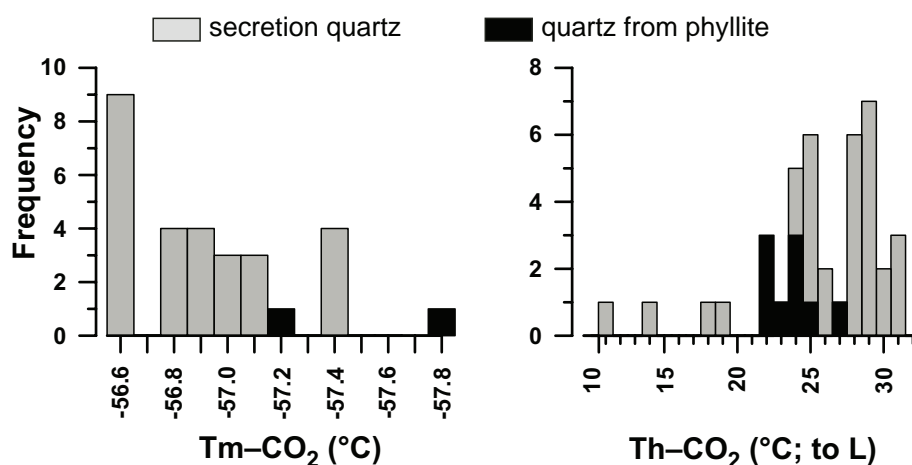
6.3. Summary of microthermometric data

6.3.1. Type I and II inclusions in the metamorphic secretion quartz

Type I and II inclusions exhibit very similar microthermometric data of the CO₂ phase: Tm–CO₂ ranges from –56.6 to –57.4 °C, whereby most of the data are clustered at –56.6 °C (Fig. 6). Admixture of other gases (CH₄, N₂) in the gas phase is thus very low (0 to 2 mol. %). Th–CO₂ (always to L) varies predominantly between 23 and 30.5 °C, with two peaks at 29 and 25 °C. Few data lie between 18.4 and 11.0 °C (Fig. 6). For type II inclusions, Th–CO₂ (to L) varied from 22.7 to 30.5 °C. Primary-looking type I inclusions (assemblage 11c) in quartz with a homogeneous degree of fill (F = 0.8) exhibited very uniform Th–CO₂ data (24.2 ± 0.4 °C; to L).

The temperature of clathrate dissociation (Tm–Cla: +9 to +10 °C; type I) indicates low salinity (0–3 wt. % eq. NaCl; Fig. 7). In many cases, however, we failed to measure Tm–Cla, mostly due to the small size of the inclusions. Similarly, total homogenization temperatures (Th–tot) of type I inclusions are scarce. We have not measured Th–tot of assemblages with a heterogeneous degree of fill. Inclusions from Assemblage 11c (F = 0.8; constant degree of fill; possibly parental fluid) homogenized at *c.* 300 °C, inclusions with the highest degree of fill from assemblages representing heterogeneous trapping homogenized at 220 °C (Assemblage 10) and at 165 °C (assemblages 2 and 3).

Fig. 6 Summary microthermometric characteristics of the carbonic phase (type I and II inclusions): **a** – melting temperature of solid CO₂; **b** – partial homogenization temperature (to liquid phase).



6.3.2. Type III inclusions in metamorphic secretion quartz

The temperature of the initial melting (Ti) was not recognizable. Ice melted from –3.5 to –0.4 °C (Tm–ice), corresponding to 5.7 to 0.7 wt. % eq. NaCl (Fig. 7). Final homogenization (Th–tot; to L) ranges from 148.5 to 231 °C (n = 44), with two prominent peaks, at 220 and 170 °C (Fig. 8). The former peak correlates with advanced crystallization of pyrite and possibly with the onset of cinnabar crystallization. The latter peak probably corresponds to the final stages of pyrite formation and to the main crystallization of cinnabar.

6.3.3. Type I and II inclusions in phyllite

In total, only 12 inclusions were studied; Tm–CO₂ from –57.2 to –57.8 °C (Fig. 6) indicates slightly higher admixture of CH₄/N₂ than suggested for the secretion quartz. The Th–CO₂ occurred from 21.5 to 26.1 °C (to L; n = 9), a few inclusions homogenized (Th–CO₂) to vapor (21.9 to 23.8 °C; n = 2) or via a critical mode (29.7 °C; 1 inclusion). Two aqueous–carbonic inclusions did not homogenize below 300 °C.

7. Discussion

7.1. Pressure and temperature during cinnabar and pyrite crystallization

Figure 9 summarizes the P–T evolution inferred for type II (CO₂-only) and type III (aqueous-only) inclusions. Intimate textural relationships between pyrite and cinnabar microinclusions and the studied fluid inclusions suggest that they were trapped during the final stages of sealing of various macroscopic fractures by the ore-bearing fluid. The homogenization temperatures therefore represent the

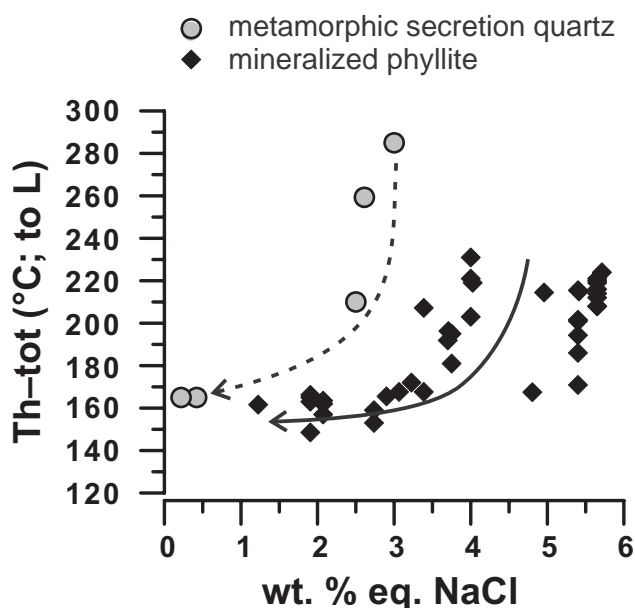


Fig. 7 Salinity versus inclusion total homogenization temperature plot. Solid and dashed lines highlight hypothetical mixing trends with low-saline (meteoric?) fluids.

minimum estimate of ore formation (i.e. slightly postdate fracture filling). The crystallization intervals of pyrite and cinnabar thus overlap significantly. Early inclusion assemblages (~220 °C), however, seem to be more pyrite-rich than the late ones (~150–160 °C). The pressure of the main ore formation is relatively well constrained by flat isochores of type II inclusions to 90–30 MPa (Fig. 9).

Metamorphic conditions for the phyllite complex at Horní Luby probably best approach type I primary inclusions in the secretion quartz lenses, for which trapping at

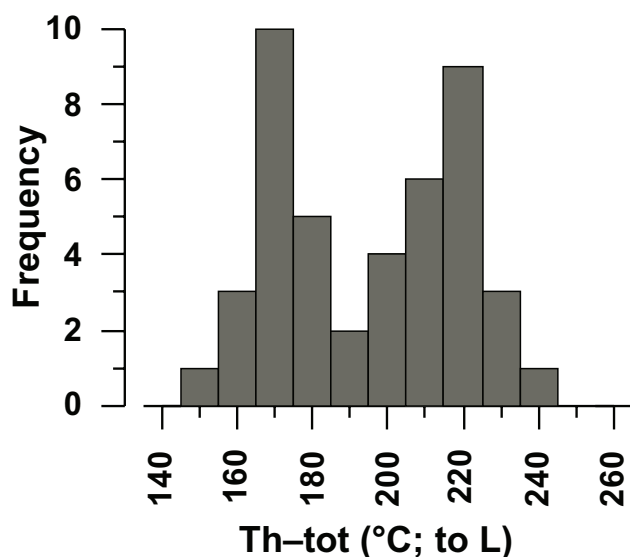


Fig. 8 Histogram of the total homogenization temperatures of fluid inclusions (inclusion types not differentiated).

~280 to ~340 °C and 300–400 MPa is assumed (Fig. 9). These data also constrain the upper theoretical limit of the formation of disseminated cinnabar ore hosted by the phyllite (i.e. the earliest ore stage). This is in good agreement with the absence of metacinnabar in the ore (based on the ore microscopy), which indicates $T < 315\text{--}345$ °C (e.g. Potter and Barnes 1978). Finally, the gaseous inclusions (type II; $\text{CO}_2 \gg \text{CH}_4$) trapped in the quartz from phyllite display densities (and Th- CO_2) similar to these of the secretion quartz lenses.

Alternatively, more complex evolution can be inferred based on the presence of sphalerite–chalcopyrite blebs/grains enclosed in cinnabar, or rimming it (Fig. 3f–g). Similar assemblage was identified at the Levigliani deposit in Alps (cinnabar II + Hg-rich sphalerite + chalcopyrite; Dini et al. 1995) where it formed at the expense of earlier zincian metacinnabar. In spite of the absence of metacinnabar at Horní Luby, the occurrence of Hg-rich sphalerite blebs in cinnabar could indicate that the zincian metacinnabar was possibly present as an earlier associated phase. However, if true, it would have to be completely replaced by Hg-rich sphalerite and cinnabar on the retrogressive path. This hypothesis could be confirmed either by finding zincian metacinnabar relics (like at Levigliani) or by determining an accurate P–T path for the host rocks at Horní Luby.

At Kraslice (about 30 km to the NE from Horní Luby), the phyllite unit contains metadiabase bodies with preserved relics of lower blueschist-facies metamorphism (350–400 °C and 600–700 MPa; Holub and Souček 1992). This temperature, at its lower range, is similar to that inferred from our fluid inclusion data (~280 to ~340 °C); the pressure is, however, much higher. The fluid inclusion data therefore seem to reflect the retrograde metamorphic conditions. Formation of cinnabar ores at < 100 MPa was probably related to the final stages of late Variscan exhumation of the Erzgebirge Complex, coeval with the late orogenic extension.

7.2. Textural and geological evidence for cinnabar and pyrite crystallization

Kulnig et al (1963) demonstrated that cinnabar mineralization at Horní Luby occurs in several horizons parallel with the metamorphic foliation. Our microscopic studies support this opinion, by largely syntectonic precipitation of disseminated cinnabar in S_1 foliation planes. We can also confirm the conclusion of Chrt and Strnad (1961) that the cinnabar replaces the metamorphic quartz.

The interval of cinnabar crystallization therefore extended from peak metamorphic (or very early retrograde) to late retrograde conditions. The richest and volumetrically most significant part of the mercury mineralization was associated with the replacement of ribbons of

metamorphic quartz by cinnabar. This process probably occurred during the early retrograde metamorphic phase as suggested by low-pressure inclusion isochores (Fig. 9) and texturally by the presence of cinnabar that fills in extensional domains (cracks and necks) in quartz-rich bands of phyllites (Fig. 2d).

7.2.1. Genetic model of the deposit

Almost all occurrences and historical cinnabar deposits within the Bohemian Massif were associated with weakly metamorphosed to unmetamorphosed Upper Ordovician to Silurian volcanosedimentary sequences (Slavíková and Slavík 1918; Sattran 1980). Volcano–hydrothermal processes connected to Lower Paleozoic volcanism were therefore the likely primary source of mercury. Individual ore bodies at various deposits display both stratiform (syngenetic?) and discordant (epigenetic) relationships to their host rocks. Mercury mobilization therefore played probably a significant role in the formation of ore bodies.

The Horní Luby district, compared to all other Czech cinnabar-mining districts, is related to the most intensely metamorphosed host-rock lithology. The deposit was originally considered to be genetically related to fluids associated with intrusions of late Variscan granites and focused by the Horní Luby Fault (Chrt and Strnad 1961). This idea was recently revised by Chrt (2001), who suggested formation by Late Paleozoic submarine volcano–exhalative processes and subsequent reworking by metamorphic processes.

More or less random distribution of mercury occurrences within the Vogtland–Saxonian Paleozoic Unit as well as the absence of a correlation between the metamorphic grade and the number of occurrences, seem to exclude large-scale

mercury mobilization/migration during the prograde phase of Variscan metamorphism. Fluid-inclusion data (this study) indicate ore (pyrite and cinnabar) formation at temperatures *c.* 100 °C lower than the anticipated local peak metamorphic conditions (~3.5 kbars, ~300 °C).

Cinnabar precipitation, ascribed to the early stage of its formation (i.e. disseminated mineralization in the phyllite) was associated with massive dissolution of the metamorphic rock-forming quartz. With respect to the suggested metamorphic conditions (~3.5 kbars, ~300 °C), we can exclude temperature-controlled retrograde solubility of quartz. The likely process that would promote massive quartz dissolution is an input of alkaline aqueous fluids. It should be noted that the mercury transport is facilitated by alkaline solutions (Potter and Barnes 1978).

With respect to the nature of the fluids and P–T conditions of ore formation, the Horní Luby district resembles the Levigliani and Ripa deposits of the Apuane Alps, Italy (Dini et al. 2001), where early ore was formed at 300–370 °C and 300–500 MPa, close to the peak metamorphism, while younger one precipitated during

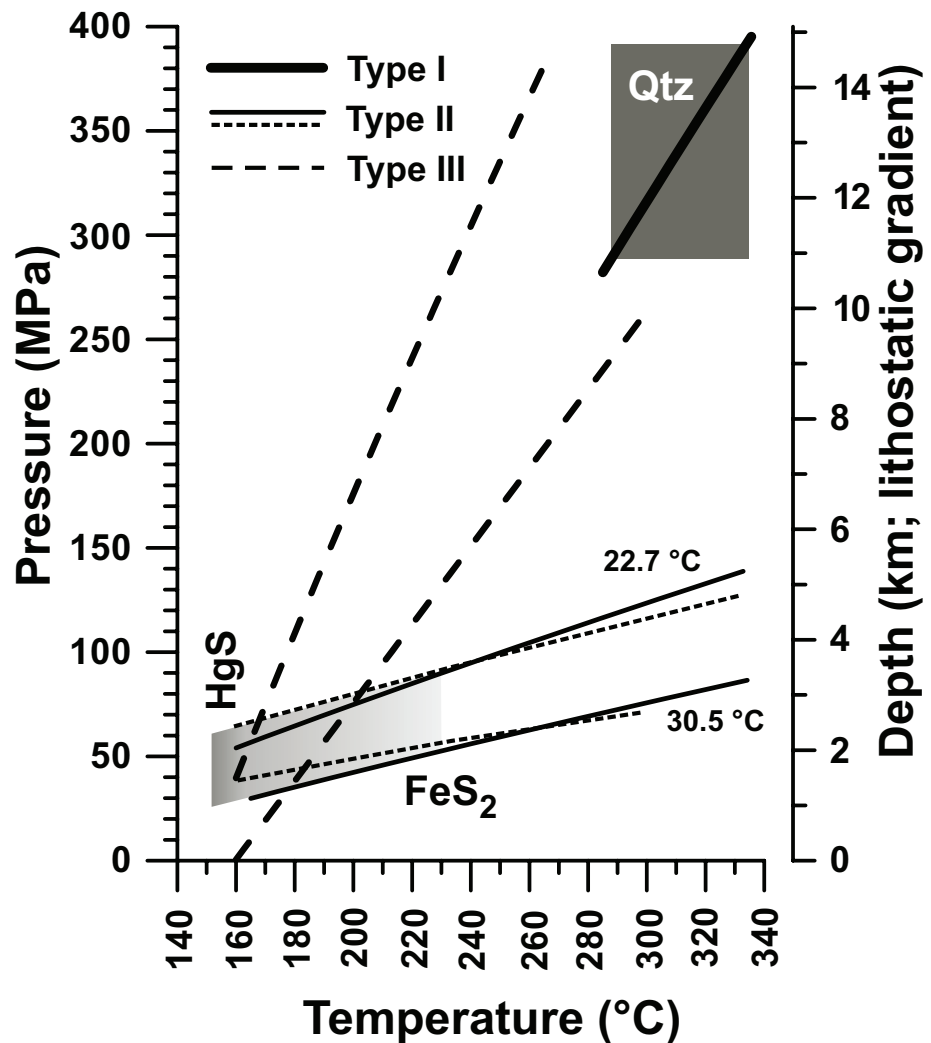


Fig. 9 Estimation of trapping conditions of the studied fluid inclusions and of ore phases. The field labeled “Qtz” corresponds to the minimum P–T conditions of the metamorphic secretion quartz formation. The field HgS–FeS₂ approximates the trapping conditions of ore phases and pyrite at higher temperature than cinnabar.

the retrograde stage (<250–150 °C). Cinnabar deposits worldwide frequently exhibit fluid inclusion homogenization temperatures within the 150–230 °C range; e.g.: Idrija in Slovenia 160–218 °C and 2.6–12.8 wt. % eq. NaCl (Palinkaš et al. 2001; Lavrič and Spanberg 2003), Almaden in Spain 375 to 85 °C, mode 220 °C, 1–13 wt. % eq. NaCl (Hernández et al. 1999) and New Idria in USA, <160 °C (Boctor et al. 1987).

8. Conclusions

The stratiform mercury deposit at Horní Luby near Cheb (Czech Republic), hosted by Ordovician phyllites of the Vogtland–Saxony Paleozoic Unit (the Saxothuringian Zone), exhibits a strong evidence for metamorphic origin and recrystallization. The ore is represented by cinnabar and pyrite disseminated within the phyllite and by bodies (lenses) containing massive cinnabar. The major mercury-bearing mineral, cinnabar, is pure, i.e. free of admixtures (Bi, Sb, Zn, Fe, Cu) and only accompanied by minute blebs of a Hg-bearing sphalerite (11–12 wt. % Hg).

Three types of fluid (aqueous–carbonic, aqueous-only, carbonic-only) were trapped in phyllites and in the secretion quartz. Early inclusions are represented by a homogeneous aqueous-carbonic metamorphic fluid ($\text{H}_2\text{O}-\text{CO}_2 \ll \text{CH}_4$) trapped at *c.* 300–350 °C and 300–400 MPa (secretion quartz formation). This fluid underwent phase heterogenization on cooling from ~300 °C down to ~200 °C. Fluid inclusions with variable gas/liquid ratios frequently contain accidentally trapped ore (mostly pyrite, less cinnabar). We suggest ore precipitation from *c.* 220–210 °C (pyrite) down to 195–160 °C (cinnabar). The pyrite–cinnabar mineralization is associated with much lower trapping pressure (~100 MPa) than peak metamorphic conditions (300–400 MPa) of the phyllite host-rock. This underlines the late metamorphic–retrograde nature of mercury-bearing fluids. The quite common replacement of metamorphic quartz in phyllite by the cinnabar was explained by the weakly alkaline nature of the mineralizing solutions.

Presence of minute blebs of Hg-rich sphalerite in cinnabar could indicate that the zincian metacinnabar was possibly present as an earlier phase in the disseminated ore; however, it was completely replaced by Hg-rich sphalerite and cinnabar during the retrogressive path. This might indicate precipitation of the earliest ore at close to the local peak metamorphic conditions (>300 °C, 300–400 MPa).

Acknowledgements. This paper benefited from internal research grant of the National Museum in Prague. We also greatly acknowledge the institutional support of Ministry of Culture of the Czech Republic to the National Museum

(DKRVO 00023272) and of Ministry of Education of the Czech Republic to the Faculty of Science, Charles University (MSM 0021620855). Radek Škoda (Masaryk University, Brno) and Martin Racek (Charles University, Prague) are thanked for assistance with electron microscope imaging and microprobe analyses. Finally, we greatly appreciate the careful review and comments by journal referees Andrea Dini and Pablo Higuera.

References

- AKÇAY M, ÖZKAN HM, MOON CJ, SPIRO B (2006) Geology, mineralogy and geochemistry of the gold-bearing stibnite and cinnabar deposits in the Emirli and Halıköy areas (Ödemiş, İzmir, West Turkey). *Ore Geol Rev* 29: 19–51
- BAKKER RJ (1997) Clathrates: computer programs to calculate fluid inclusion V–X properties using clathrate melting temperatures. *Comput Geosci* 23: 1–18
- BAKKER RJ (1999) Adaptation of the Bowers and Helgeson (1983) equation of state to the $\text{H}_2\text{O}-\text{CO}_2-\text{CH}_4-\text{N}_2-\text{NaCl}$ system. *Chem Geol* 154: 225–236
- BÍLEK J, JANGL L, URBAN J (1978a) History of mining: Cheb area. Unpublished report (Geofond Praha, P 28588), pp 145–199 (in Czech)
- BÍLEK J, JANGL L, URBAN J (1978b) History of cinnabar and mercury mining in the Bohemian Massif. Unpublished report (ČGS, C865; Geofond Praha P 26271), pp 1–59
- BOCTOR NZ, SHIEH YN, KULLERUD G (1987) Mercury ores from the New Idria Mining District, California: geochemical and stable isotope studies. *Geochim Cosmochim Acta* 51: 1705–1715
- BODNAR RJ (1993) Revised equation and table for determining the freezing point depression of $\text{H}_2\text{O}-\text{NaCl}$ solutions. *Geochim Cosmochim Acta* 57: 683–684
- CHRT J (1972) Mercury deposits in the Bohemian Massif. *Geol Průzk* 14: 315 (in Czech)
- CHRT J (2001) Lower Paleozoic stratiform ore deposits of Erzgebirge and Fichtelgebirge Mts. Uhlí, Rudy 49, *Geol Průzk* 43: 3–10 (in Czech)
- CHRT J, STRNAD J (1961) Geology of the cinnabar deposit at Horní Luby west of Kraslice. *Čas Mineral Geol* 6: 18–30 (in Czech)
- DINI A, BENVENUTI M, LATTANZI P, TANELLI G (1995) Mineral assemblages in the Hg–Zn–(Fe)–S system at Levigliani, Tuscany, Italy. *Eur J Mineral* 7: 417–427
- DINI A, BENVENUTI M, COSTAGLIOLA P, LATTANZI P (2001) Mercury deposits in metamorphic settings: the example of Levigliani and Ripa mines, Apuane Alps (Tuscany, Italy). *Ore Geol Rev* 18: 149–167
- FALK F, FRANKE W, KURZE M (1995) V. Saxothuringian Basin, V. B. Autochthon and nonmetamorphic nappe units. V. B. 1. Stratigraphy. In: DALLMEYER RD, FRANKE

- W, WEBER K (eds) Pre-Permian Geology of Central and Eastern Europe. Springer, Berlin, pp 221–234
- FARYAD SW, KACHLÍK V (2013) New evidence of blueschist facies rocks and their geotectonic implication for Variscan suture(s) in the Bohemian Massif. *J Metamorph Geol* 31: 63–82
- HAMPTON WA, WHITE GP, HOSKIN PWO, BROWNE PRL, RODGERS KA (2004) Cinnabar, livingstonite, stibnite and pyrite in Pliocene silica sinter from Northland, New Zealand. *Mineral Mag* 68: 191–198
- HAZEN RM, GOLDEN J, DOWNS RT, HYSTAD G, GREW ES, AZZOLINI D, SVERJENSKY DA (2012) Mercury (Hg) mineral evolution: a mineralogical record of supercontinent assembly, changing ocean geochemistry, and the emerging terrestrial biosphere. *Amer Miner* 97: 1013–1042
- HERNÁNDEZ A, JÉBRAK M, HIGUERAS P, OYARZUN R, MORATA D, MUNHA J (1999) The Almadén mercury mining district, Spain. *Miner Depos* 34: 539–548
- HOLUB FV, SOUČEK J (1992) Blueschist–greenschist metamorphism of metabasites in the western Krušné Hory (Erzgebirge) Mts. *Zbl Geol Paläont Teil I* 7/8: 815–826
- JÉBRAK M, HERNANDEZ A (1995) Tectonic deposition of mercury in the Almadén district, Las Cuevas deposit, Spain. *Miner Depos* 30: 413–423
- KLIER R (1969) Der Konkurrenzkampf zwischen dem böhmischen und dem idrianischen Quecksilber in der ersten Hälfte des 16. Jahrhunderts. *Bohemia: Jb Colleg Carolinum* 8: 82–110 (in German)
- KONOPÁSEK J, SCHULMANN K (2005) Contrasting Early Carboniferous field geotherms: evidence for accretion of a thickened orogenic root and subducted Saxothuringian crust (Central European Variscides). *J Geol Soc London* 162: 463–470
- KOŘAN J (1942) History of mercury. *Horn Věst Horn hutn Listy* (Praha) 24 (43): 29–35 (in Czech)
- KULNIG E, MACEVIČ V, KAUTSKÝ J, STRNAD J (1963) Horní Luby, exploration for Hg-ores 1961–1962. Unpublished report (Geofond Praha P 15358), pp 1–50
- LAVRIČ JV, SPANGENBERG JE (2003) Stable isotope (C, O, S) systematics of the mercury mineralization at Idrija, Slovenia: constraints on fluid source and alteration processes. *Miner Depos* 38: 886–899
- LORENZ W (1989) Geological outline of the Erzgebirge Anticlinorium. In: TISCHENDORF G (ed) *Silicic magmatism and metallogenesis of the Erzgebirge*. *Veröff Zentr-Inst Phys Erde* (Berlin) 107: 6–34
- LÖWL K (1908) Dějiny výroby kovů v Čechách. *Horn hutn Listy* 9: 67–69 (in Czech)
- MARTÍN-IZARD A, GUMIEL P, ARIAS M, CEPEDAL A, FUERTES-FUENTE M, REGUILÓN R (2009) Genesis and evolution of the structurally controlled vein mineralization (Sb–Hg) in the Escarlati deposit (León, Spain): evidence from fault population analysis methods, fluid-inclusion research and stable isotope data. *J Geochem Explor* 100: 51–66
- MAUCHER A (1976) The strata-bound cinnabar–stibnite–scheelite deposits (discussed with examples from Mediterranean region). In: WOLF KH (ed) *Handbook of Strata-bound and Stratiform Ore Deposits. II. Regional Studies and Specific Deposits. Vol. 7*. Elsevier, Amsterdam, pp 477–503
- PALINKAŠ LA, STRMIČ S, HERLEC U (2001) The ore-forming fluids in the Idrija mercury mine, Slovenia. In: PIESTRZYŃSKI et al. (eds) *Mineral Deposits at the Beginning of the 21st Century*. Swets & Zeitlinger, Lisse, pp 321–324
- PERTOLD Z, CHRT J, BUDIL V, BURDA P, BURDOVÁ P, KRÍBEK B, PERTOLDOVÁ J, GASKARTH B (1994) The Tisová Cu-deposit: a Beshi-type in the Krušné hory Mts., Bohemian Massif, Czech Republic. *Monograph Series on Mineral Deposits*. Gebrüder Borntraeger, Berlin–Stuttgart, 31: 71–95
- POTTER RWII, BARNES HL (1978) Phase relations in the binary Hg–S. *Amer Miner* 63: 1143–1152
- RÖTZLER K, SCHUMACHER R, MARESCH VW, WILLNER AP (1998) Characterization and geodynamic implications of contrasting metamorphic evolution in juxtaposed high-pressure units of the Western Erzgebirge (Saxony, Germany). *Eur J Mineral* 10: 261–280
- SAUPÉ F (1990) Geology of the Almadén mercury deposit, Province of Ciudad Real, Spain. *Econ Geol* 85: 482–510
- SATTRAN V (1980) Mercury mineralization hosted by Lower Paleozoic volcanosedimentary sequences in the Bohemian Massif. *Sbor geol Věd, Lož Geol Mineral* 21: 101–131 (in Czech)
- SATTRAN V, ŠKVOR V (1962) Report on geological mapping of crystalline complexes at map sheets Luby and Krásná. *Zpr geol Výzk za R 1962* 16–19 (in Czech)
- SATTRAN V, MAŇOUR J, ODEHNAL L, PTÁK J, ZIMA L (1978) Regional prognosis of Hg-mineralization in the Bohemian Massif. Unpublished report, Czech Geological Survey, Prague, pp 1–137 (in Czech)
- SCHUEFELE G (1940) About the cinnabar mining at Niederschlaue, Hartenstein and Schönbach. Unpublished MSc thesis, Bergakademie Freiberg, pp 1–65 (in German)
- SCHULZ H (1965) Mercury mineralisation in southern part of Geraer Forland (Thüringen). *Bergakademie* (Freiber) 27: 445–452 (in German)
- SLAVÍKOVÁ L, SLAVÍK F (1918) Iron ores from Lower Silurian in Bohemia. *Rozpr Čes Akad Vědy Slovesn Umění, Tř II* 26: 1–60 (in Czech)
- SMITH CN, KESLER SE, BLUM JD, RYTUBA JJ (2008) Isotope geochemistry of mercury in source rocks, mineral deposits and spring deposits of the California Coast Ranges, USA. *Earth Planet Sci Lett* 269: 399–407
- STUDEMEISTER PA (1984) Mercury deposits of western California: an overview. *Miner Depos* 19: 202–207
- TISCHENDORF G (1989) Sb–Au–Hg depositions related with Hercynian postkinematic granitoid complexes.

- In: TISCHENDORF G (ed) *Silicic Magmatism and Metallogeneses of the Erzgebirge*. Veröff Zentr-Inst Phys Erde (Berlin) 107: 108–110
- THIERY R, VAN DEN KERKHOF AM, DUBESSY J (1994) vX properties of CH₄-CO₂ and CO₂-N₂ fluid inclusions: modeling for T < 31°C and P < 400 bars. *Eur J Mineral* 6: 753–771
- VELEBIL D (2009) Cinnabar mining in Horní Luby (Ober Schönbach) near Cheb (Eger), Czech Republic. *Bull mineral-petrolog Odd Nár Muz (Praha)* 17: 39–61 (in Czech)
- WHITE DE (1981) Active geothermal systems and hydrothermal ore deposits. *Econ Geol*, 75th Anniv Vol: 392–423
- ZHANG YG, FRANTZ JD (1987) Determination of the homogenization temperatures and densities of supercritical fluids in the system NaCl-KCl-CaCl₂-H₂O using synthetic fluid inclusions. *Chem Geol* 64: 335–350